8
INTERNAL FLOW ENERGY CONVERSION

8.1 INTRODUCTION

One of the most common requirements of a multiphase flow analysis is the prediction of the energy gains and losses as the flow proceeds through the pipes, valves, pumps, and other components that make up an internal flow system. In this chapter we will attempt to provide a few insights into the physical processes that influence these energy conversion processes in a multiphase flow. The literature contains a plethora of engineering correlations for pipe friction and some data for other components such as pumps. This chapter will provide an overview and some references to illustrative material, but does not pretend to survey these empirical methodologies.

As might be expected, frictional losses in straight uniform pipe flows have been the most widely studied of these energy conversion processes and so we begin with a discussion of that subject, focusing first on disperse or nearly disperse flows and then on separated flows. In the last part of the chapter, we consider multiphase flows in pumps, in part because of the ubiquity of these devices and in part because they provide a second example of the multiphase flow effects in internal flows.

8.2 FRICTIONAL LOSS IN DISPERSE FLOW

8.2.1 Horizontal Flow

We begin with a discussion of disperse horizontal flow. There exists a substantial body of data relating to the frictional losses or pressure gradient, $(-dp/ds)$, in a straight pipe of circular cross-section (the coordinate s is measured along the axis of the pipe). Clearly $(-dp/ds)$ is a critical factor in the design of many systems, for example slurry pipelines. Therefore a substantial data base exists for the flows of mixtures of solids and water

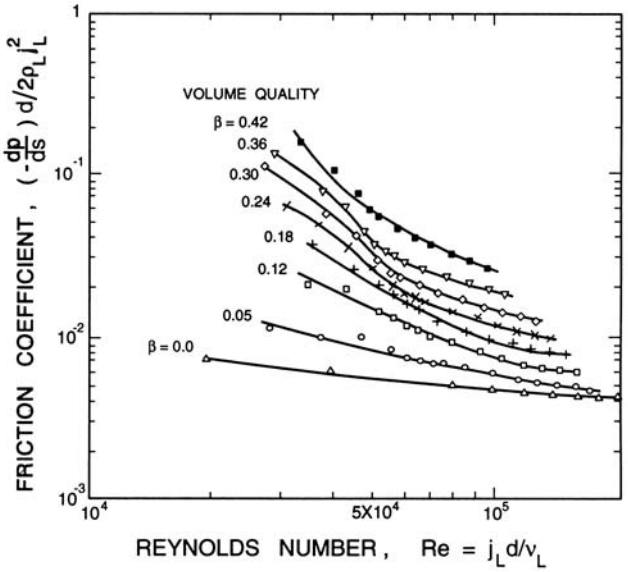

Figure 8.1. Typical friction coefficients (based on the liquid volumetric flux and the liquid density) plotted against Reynolds number (based on the liquid volumetric flux and the liquid viscosity) for the horizontal pipeline flow ($d = 5.2cm$) of sand ($D = 0.018cm$) and water at $21°C$ (Lazarus and Neilson 1978).

in horizontal pipes. The hydraulic gradient is usually non-dimensionalized using the pipe diameter, d, the density of the suspending phase (ρ_L if liquid), and either the total volumetric flux, j, or the volumetric flux of the suspending fluid (j_L if liquid). Thus, commonly used friction coefficients are

$$C_f = \frac{d}{2\rho_L j_L^2}\left(-\frac{dp}{ds}\right) \quad \textbf{or} \quad C_f = \frac{d}{2\rho_L j^2}\left(-\frac{dp}{ds}\right) \tag{8.1}$$

and, in parallel with the traditional Moody diagram for single phase flow, these friction coefficients are usually presented as functions of a Reynolds number for various mixture ratios as characterized by the volume fraction, α, or the volume quality, β, of the suspended phase. Commonly used Reynolds numbers are based on the pipe diameter, the viscosity of the suspending phase (ν_L if liquid) and either the total volumetric flux, j, or the volumetric flux of the suspending fluid.

For a more complete review of slurry pipeline data the reader is referred to Shook and Roco (1991) and Lazarus and Neilsen (1978). For the solids/gas flows associated with the pneumatic conveying of solids, Soo (1983) provides a good summary. For boiling flows or for gas/liquid flows, the reader is

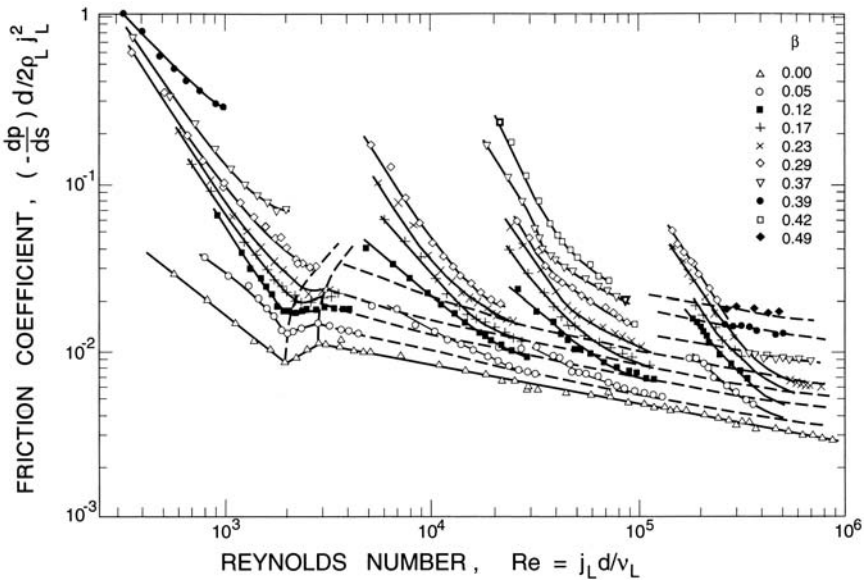

Figure 8.2. Typical friction coefficients (based on the liquid volumetric flux and the liquid density) plotted against Reynolds number (based on the liquid volumetric flux and the liquid viscosity) for the horizontal pipeline flow of four different solid/liquid mixtures (Lazarus and Neilson 1978).

referred to the reviews of Hsu and Graham (1976) and Collier and Thome (1994).

The typical form of the friction coefficient data is illustrated in figures 8.1 and 8.2 taken from Lazarus and Neilson (1978). Typically the friction coefficient increases markedly with increasing concentration and this increase is more significant the lower the Reynolds number. Note that the measured increases in the friction coefficient can exceed an order of magnitude. For a given particle size and density, the flow in a given pipe becomes increasingly homogeneous as the flow rate is increased since, as discussed in section 7.3.1, the typical mixing velocity is increasing while the typical segregation velocity remains relatively constant. The friction coefficient is usually increased by segregation effects, so, for a given pipe and particles, part of the decrease in the friction coefficient with increasing flow rate is due to the normal decrease with Reynolds number and part is due to the increasing homogeneity of the flow. Figure 8.2, taken from Lazarus and Neilson, shows how the friction coefficient curves for a variety of solid-liquid flows, tend to asymptote at higher Reynolds numbers to a family of curves (shown by the dashed lines) on which the friction coefficient is a function only of the Reynolds number and volume fraction. These so-called *base curves* pertain

when the flow is sufficiently fast for complete mixing to occur and the flow regime becomes homogeneous. We first address these base curves and the issue of homogeneous flow friction. Later, in section 8.2.3, we comment on the departures from the base curves that occur at lower flow rates when the flow is in the heterogeneous or saltation regimes.

8.2.2 Homogeneous flow friction

When the multiphase flow or slurry is thoroughly mixed the pressure drop can be approximated by the friction coefficient for a single-phase flow with the mixture density, ρ (equation 1.8) and the same total volumetric flux, $j = j_S + j_L$, as the multiphase flow. We exemplify this using the slurry pipeline data from the preceding section assuming that $\alpha = \beta$ (which does tend to be the case in horizontal homogeneous flows) and setting $j = j_L/(1-\alpha)$. Then the ratio of the base friction coefficient at finite loading, $C_f(\alpha)$, to the friction coefficient for the continuous phase alone, $C_f(0)$, should be given by

$$\frac{C_f(\alpha)}{C_f(0)} = \frac{(1+\alpha\rho_S/\rho_L)}{(1-\alpha)^2} \tag{8.2}$$

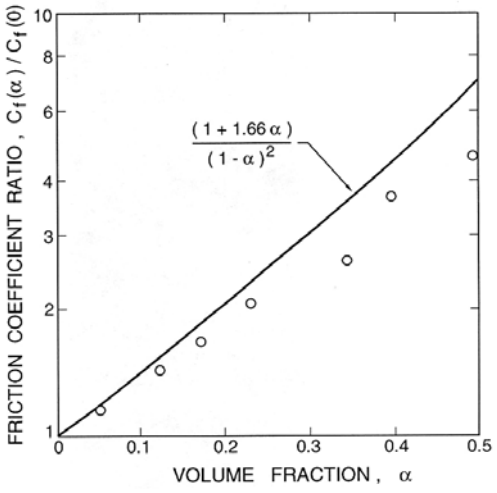

Figure 8.3. The ratio of the *base curve* friction coefficient at finite loading, $C_f(\alpha)$, to the friction coefficient for the continuous phase alone, $C_f(0)$. Equation 8.2 (line) is compared with the data of Lazarus and Neilsen (1978).

A comparison between this expression and the data from the base curves of Lazarus and Neilsen is included in figure 8.3 and demonstrates a reasonable agreement.

Thus a flow regime that is homogeneous or thoroughly mixed can usually be modeled as a single phase flow with an effective density, volume flow rate and viscosity. In these circumstances the orientation of the pipe appears to make little difference. Often these correlations also require an effective mixture viscosity. In the above example, an effective kinematic viscosity of the multiphase flow could have been incorporated in the expression 8.2; however, this has little effect on the comparison in figure 8.3 especially under the turbulent conditions in which most slurry pipelines operate.

Wallis (1969) includes a discussion of homogeneous flow friction correlations for both laminar and turbulent flow. In laminar flow, most correlations use the mixture density as the effective density and the total volumetric flux, j, as the velocity as we did in the above example. A wide variety of mostly empirical expressions are used for the effective viscosity, μ_e. In low volume fraction suspensions of solid particles, Einstein's (1906) classical effective viscosity given by

$$\mu_e = \mu_C(1 + 5\alpha/2) \tag{8.3}$$

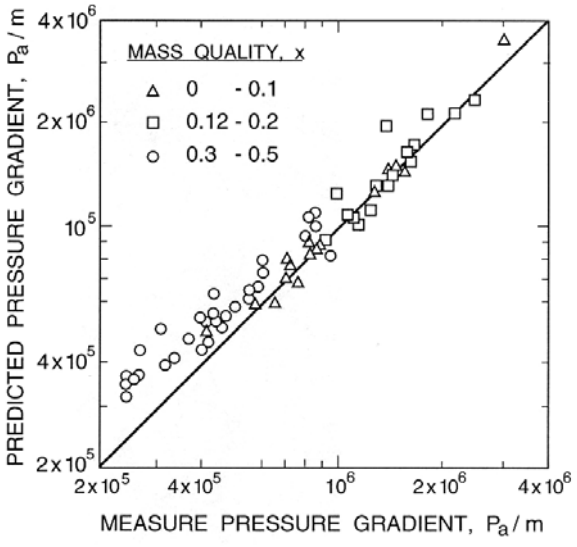

Figure 8.4. Comparison of the measured friction coefficient with that using the homogeneous prediction for steam/water flows of various mass qualities in a $0.3cm$ diameter tube. From Owens (1961).

is appropriate though this expression loses validity for volume fractions greater than a few percent. In emulsions with droplets of viscosity, μ_D, the extension of Einstein's formula,

$$\mu_e = \mu_C \left\{ 1 + \frac{5\alpha}{2} \frac{(\mu_D + 2\mu_C/5)}{(\mu_D + \mu_C)} \right\} \tag{8.4}$$

is the corresponding expression (Happel and Brenner 1965). More empirical expressions for μ_e are typically used at higher volume fractions.

As discussed in section 1.3.1, turbulence in multiphase flows introduces another set of complicated issues. Nevertheless as was demonstrated by the above example, the effective single phase approach to pipe friction seems to produce moderately accurate results in homogeneous flows. The comparison in figure 8.4 shows that the errors in such an approach are about $\pm 25\%$. The presence of particles, particularly solid particles, can act like surface roughness, enhancing turbulence in many applications. Consequently, turbulent friction factors for homogeneous flow tend to be similar to the values obtained for single phase flow in rough pipes, values around 0.005 being commonly experienced (Wallis 1969).

8.2.3 Heterogeneous flow friction

The most substantial remaining issue is to understand the much larger friction factors that occur when particle segregation predominates. For example, commenting on the data of figure 8.2, Lazarus and Neilsen show that values larger than the base curves begin when component separation begins to occur and the flow regime changes from the heterogeneous regime to the saltation regime (section 7.2.3 and figure 7.5). Another slurry flow example is shown in figure 8.5. According to Hayden and Stelson (1971) the minima in the fitted curves correspond to the boundary between the heterogeneous and saltation flow regimes. Note that these all occur at essentially the same critical volumetric flux, j_c; this agrees with the criterion of Newitt *et al.* (1955) that was discussed in section 7.3.1 and is equivalent to a critical volumetric flux, j_c, that is simply proportional to the terminal velocity of individual particles and independent of the loading or mass fraction.

The transition of the flow regime from heterogeneous to saltation results in much of the particle mass being supported directly by particle contacts with the interior surface of the pipe. The frictional forces that this contact produces implies, in turn, a substantial pressure gradient in order to move the bed. The pressure gradient in the moving bed configuration can be readily estimated as follows. The submerged weight of solids in the packed bed

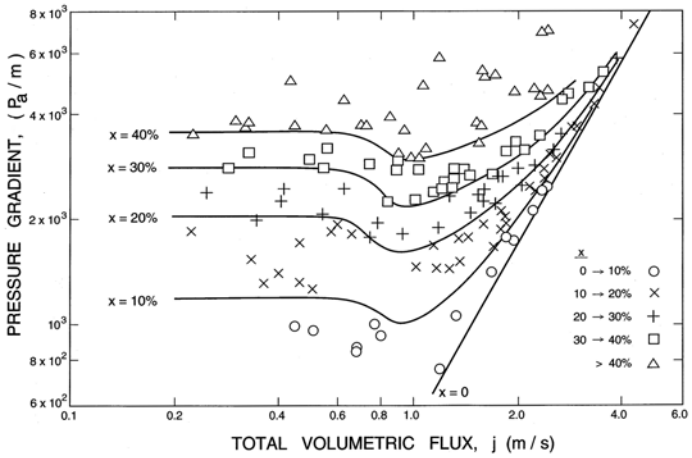

Figure 8.5. Pressure gradients in a $2.54cm$ diameter horizontal pipeline plotted against the total volumetric flux, j, for a slurry of sand with particle diameter $0.057cm$. Curves for four specific mass fractions, x (in percent) are fitted to the data. Adapted from Hayden and Stelson (1971).

per unit length of the cylindrical pipe of diameter, d, is

$$\pi d^2 \alpha g(\rho_S - \rho_L) \tag{8.5}$$

where α is the overall effective volume fraction of solids. Therefore, if the effective Coulomb friction coefficient is denoted by η, the longitudinal force required to overcome this friction per unit length of pipe is simply η times the above expression. The pressure gradient needed to provide this force is therefore

$$-\left(\frac{dp}{ds}\right)_{friction} = \eta \alpha g(\rho_S - \rho_L) \tag{8.6}$$

With η considered as an adjustable constant, this is the expression for the additional frictional pressure gradient proposed by Newitt *et al.* (1955). The final step is to calculate the volumetric flow rate that occurs with this pressure gradient, part of which proceeds through the packed bed and part of which flows above the bed. The literature contains a number of semi-empirical treatments of this problem. One of the first correlations was that of Durand and Condolios (1952) that took the form

$$j_c = f(\alpha, D)\left\{2gd\frac{\Delta\rho}{\rho_L}\right\}^{\frac{1}{2}} \tag{8.7}$$

where $f(\alpha, D)$ is some function of the solids fraction, α, and the particle

diameter, D. There are both similarities and differences between this expression and that of Newitt *et al.* (1955). A commonly used criterion that has the same form as equation 8.7 but is more specific is that of Zandi and Govatos (1967):

$$j_c = \left\{ \frac{K\alpha dg}{C_D^{\frac{1}{2}}} \frac{\Delta\rho}{\rho_L} \right\}^{\frac{1}{2}} \tag{8.8}$$

where K is an empirical constant of the order of $10 - 40$. Many other efforts have been made to correlate the friction factor for the heterogeneous and saltation regimes; reviews of these mostly empirical approaches can be found in Zandi (1971) and Lazarus and Neilsen (1978). Fundamental understanding is less readily achieved; perhaps future understanding of the granular flows described in chapter 13 will provide clearer insights.

8.2.4 Vertical flow

As indicated by the flow regimes of section 7.2.2, vertically-oriented pipe flow can experience partially separated flows in which large relative velocities develop due to buoyancy and the difference in the densities of the two-phases or components. These large relative velocities complicate the problem of evaluating the pressure gradient. In the next section we describe the traditional approach used for separated flows in which it is assumed that the phases or components flow in separate but communicating streams. However, even when the multiphase flow has a solid particulate phase or an incompletely separated gas/liquid mixture, partial separation leads to friction factors that exhibit much larger values than would be experienced in a homogeneous flow. One example of that in horizontal flow was described in section 8.2.1. Here we provide an example from vertical pipe flows. Figure 8.6 contains friction factors (based on the total volumetric flux and the liquid density) plotted against Reynolds number for the flow of air bubbles and water in a $10.2cm$ vertical pipe for three ranges of void fraction. Note that these are all much larger than the single phase friction factor. Figure 8.7 presents further details from the same experiments, plotting the ratio of the frictional pressure gradient in the multiphase flow to that in a single phase flow of the same liquid volumetric flux against the volume quality for several ranges of Reynolds number. The data shows that for small volume qualities the friction factor can be as much as an order of magnitude larger than the single phase value. This substantial effect decreases as the Reynolds number increases and also decreases at higher volume fractions. To emphasize the

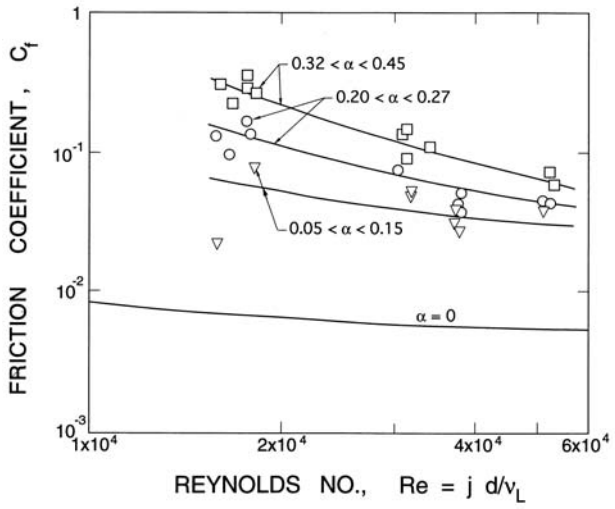

Figure 8.6. Typical friction coefficients (based on total volumetric flux and the liquid density) plotted against Reynolds number (based on the total volumetric flux and the liquid viscosity) for the flow of air bubbles and water in a $10.2cm$ vertical pipe flow for three ranges of air volume fraction, α, as shown (Kytömaa 1987).

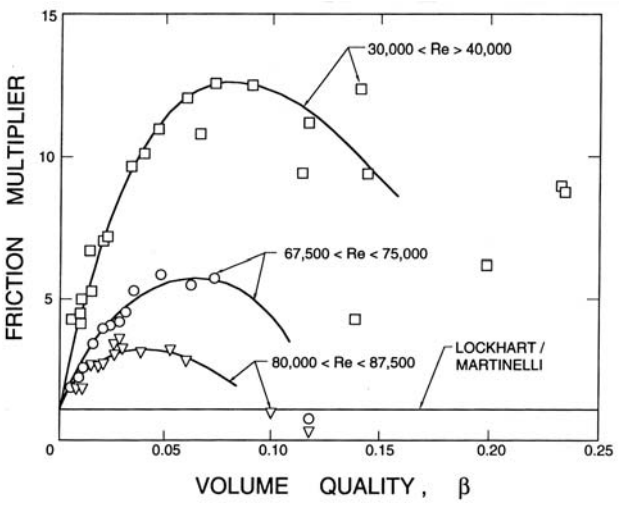

Figure 8.7. Typical friction multiplier data (defined as the ratio of the actual frictional pressure gradient to the frictional pressure gradient that would occur for a single phase flow of the same liquid volume flux) for the flow of air bubbles and water in a $10.2cm$ vertical pipe plotted against the volume quality, β, for three ranges of Reynolds number as shown (Kytömaa 1987).

importance of this phenomenon in partially separated flows, a line representing the Lockhart-Martinelli correlation for fully separated flow (see section 8.3.1) is also included in figure 8.7. As in the case of partially separated horizontal flows discussed in section 8.2.1, there is, as yet, no convincing explanation of the high values of the friction at lower Reynolds numbers. But the effect seems to be related to the large unsteady motions caused by the presence of a disperse phase of different density and the effective stresses (similar to Reynolds stresses) that result from the inertia of these unsteady motions.

8.3 FRICTIONAL LOSS IN SEPARATED FLOW

Having discussed homogeneous and disperse flows we now turn our attention to the friction in separated flows and, in particular, describe the commonly used Martinelli correlations.

8.3.1 Two component flow

The Lockhart-Martinelli and Martinelli- Nelson correlations attempt to predict the frictional pressure gradient in two-component or two-phase flows in pipes of constant cross-sectional area, A. It is assumed that these multiphase flows consist of two separate co-current streams that, for convenience, we will refer to as the liquid and the gas though they could be any two immiscible fluids. The correlations use the results for the frictional pressure gradient in single phase pipe flows of each of the two fluids. In two-phase flow, the volume fraction is often changing as the mixture progresses along the pipe and such phase change necessarily implies acceleration or deceleration of the fluids. Associated with this acceleration is an acceleration component of the pressure gradient that is addressed in a later section dealing with the Martinelli-Nelson correlation. Obviously, it is convenient to begin with the simpler, two-component case (the Lockhart-Martinelli correlation); this also neglects the effects of changes in the fluid densities with distance, s, along the pipe axis so that the fluid velocities also remain invariant with s. Moreover, in all cases, it is assumed that the hydrostatic pressure gradient has been accounted for so that the only remaining contribution to the pressure gradient, $-dp/ds$, is that due to the wall shear stress, τ_w. A simple balance of forces requires that

$$-\frac{dp}{ds} = \frac{P}{A}\tau_w \tag{8.9}$$

where P is the perimeter of the cross-section of the pipe. For a circular pipe, $P/A = 4/d$, where d is the pipe diameter and, for non-circular cross-sections, it is convenient to define a *hydraulic diameter*, $4A/P$. Then, defining the dimensionless friction coefficient, C_f, as

$$C_f = \tau_w / \frac{1}{2}\rho j^2 \tag{8.10}$$

the more general form of equation 8.1 becomes

$$-\frac{dp}{ds} = 2C_f \rho j^2 \frac{P}{4A} \tag{8.11}$$

In single phase flow the coefficient, C_f, is a function of the Reynolds number, $\rho dj/\mu$, of the form

$$C_f = \mathcal{K} \left\{ \frac{\rho dj}{\mu} \right\}^{-m} \tag{8.12}$$

where $\mathcal{K}$ is a constant that depends on the roughness of the pipe surface and will be different for laminar and turbulent flow. The index, m, is also different, being 1 in the case of laminar flow and $\frac{1}{4}$ in the case of turbulent flow.

These relations from single phase flow are applied to the two cocurrent streams in the following way. First, we define hydraulic diameters, d_L and d_G, for each of the two streams and define corresponding area ratios, κ_L and κ_G, as

$$\kappa_L = 4A_L/\pi d_L^2 \quad ; \quad \kappa_G = 4A_G/\pi d_G^2 \tag{8.13}$$

where $A_L = A(1-\alpha)$ and $A_G = A\alpha$ are the actual cross-sectional areas of the two streams. The quantities κ_L and κ_G are shape parameters that depend on the geometry of the flow pattern. In the absence of any specific information on this geometry, one might choose the values pertinent to streams of circular cross-section, namely $\kappa_L = \kappa_G = 1$, and the commonly used form of the Lockhart-Martinelli correlation employs these values. However, as an alternative example, we shall also present data for the case of annular flow in which the liquid coats the pipe wall with a film of uniform thickness and the gas flows in a cylindrical core. When the film is thin, it follows from the annular flow geometry that

$$\kappa_L = 1/(1-\alpha) \quad ; \quad \kappa_G = 1 \tag{8.14}$$

where it has been assumed that only the exterior perimeter of the annular liquid stream experiences significant shear stress.

In summary, the basic geometric relations yield

$$\alpha = 1 - \kappa_L d_L^2/d^2 = \kappa_G d_G^2/d^2 \tag{8.15}$$

Then, the pressure gradient in each stream is assumed given by the following coefficients taken from single phase pipe flow:

$$C_{fL} = \mathcal{K}_L \left\{ \frac{\rho_L d_L u_L}{\mu_L} \right\}^{-m_L} \quad ; \quad C_{fG} = \mathcal{K}_G \left\{ \frac{\rho_G d_G u_G}{\mu_G} \right\}^{-m_G} \tag{8.16}$$

and, since the pressure gradients must be the same in the two streams, this imposes the following relation between the flows:

$$-\frac{dp}{ds} = \frac{2\rho_L u_L^2 \mathcal{K}_L}{d_L} \left\{ \frac{\rho_L d_L u_L}{\mu_L} \right\}^{-m_L} = \frac{2\rho_G u_G^2 \mathcal{K}_G}{d_G} \left\{ \frac{\rho_G d_G u_G}{\mu_G} \right\}^{-m_G} \tag{8.17}$$

In the above, m_L and m_G are 1 or $\frac{1}{4}$ depending on whether the stream is laminar or turbulent. It follows that there are four permutations namely:

- both streams are laminar so that $m_L = m_G = 1$, a permutation denoted by the double subscript LL
- a laminar liquid stream and a turbulent gas stream so that $m_L = 1$, $m_G = \frac{1}{4}$ (LT)
- a turbulent liquid stream and a laminar gas stream so that $m_L = \frac{1}{4}$, $m_G = 1$ (TL) and
- both streams are turbulent so that $m_L = m_G = \frac{1}{4}$ (TT)

Equations 8.15 and 8.17 are the basic relations used to construct the Lockhart-Martinelli correlation. However, the solutions to these equations are normally and most conveniently presented in non-dimensional form by defining the following dimensionless pressure gradient parameters:

$$\phi_L^2 = \frac{\left(\frac{dp}{ds}\right)_{actual}}{\left(\frac{dp}{ds}\right)_L} \quad ; \quad \phi_G^2 = \frac{\left(\frac{dp}{ds}\right)_{actual}}{\left(\frac{dp}{ds}\right)_G} \tag{8.18}$$

where $(dp/ds)_L$ and $(dp/ds)_G$ are respectively the hypothetical pressure gradients that would occur in the same pipe if only the liquid flow were present and if only the gas flow were present. The ratio of these two hypothetical gradients, Ma^2, given by

$$Ma^2 = \frac{\phi_G^2}{\phi_L^2} = \frac{\left(\frac{dp}{ds}\right)_L}{\left(\frac{dp}{ds}\right)_G} = \frac{\rho_L}{\rho_G} \frac{G_G^2}{G_L^2} \frac{\mathcal{K}_G}{\mathcal{K}_L} \frac{\left\{\frac{G_G d}{\mu_G}\right\}^{-m_G}}{\left\{\frac{G_L d}{\mu_L}\right\}^{-m_L}} \tag{8.19}$$

defines the Martinelli parameter, Ma, and allows presentation of the solutions to equations 8.15 and 8.17 in a convenient parametric form. Using the

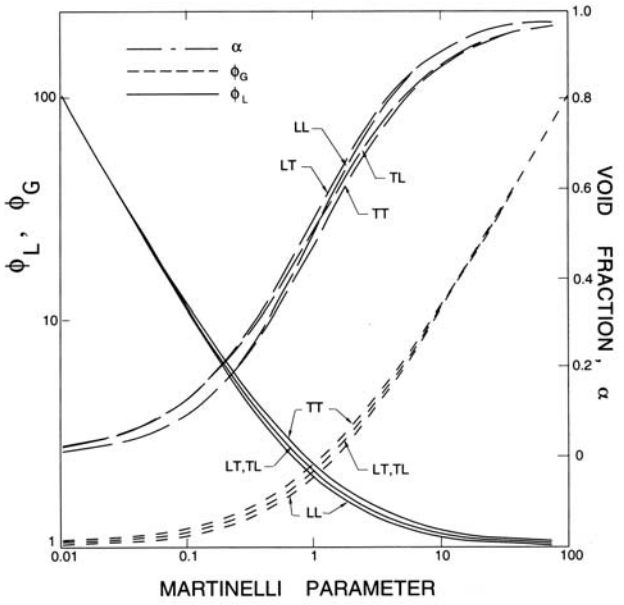

Figure 8.8. The Lockhart-Martinelli correlation results for ϕ_L and ϕ_G and the void fraction, α, as functions of the Martinelli parameter, Ma, for the case, $\kappa_L = \kappa_G = 1$. Results are shown for the four laminar and turbulent stream permutations, LL, LT, TL and TT.

definitions of equations 8.18, the non-dimensional forms of equations 8.15 become

$$\alpha = 1 - \kappa_L^{-(1+m_L)/(m_L-5)} \phi_L^{4/(m_L-5)} = \kappa_G^{-(1+m_G)/(m_G-5)} \phi_G^{4/(m_G-5)} \qquad (8.20)$$

and the solution of these equations produces the Lockhart-Martinelli prediction of the non-dimensional pressure gradient.

To summarize: for given values of

- the fluid properties, ρ_L, ρ_G, μ_L and μ_G
- a given type of flow LL, LT, TL or TT along with the single phase correlation constants, m_L, m_G, $\mathcal{K}_L$ and $\mathcal{K}_G$
- given values or expressions for the parameters of the flow pattern geometry, κ_L and κ_G
- and a given value of α

equations 8.20 can be solved to find the non-dimensional solution to the flow, namely the values of ϕ_L^2 and ϕ_G^2. The value of Ma^2 also follows and the rightmost expression in equation 8.19 then yields a relation between the liquid mass flux, G_L, and the gas mass flux, G_G. Thus, if one is also given just **one** mass flux (often this will be the total mass flux, G), the solution will

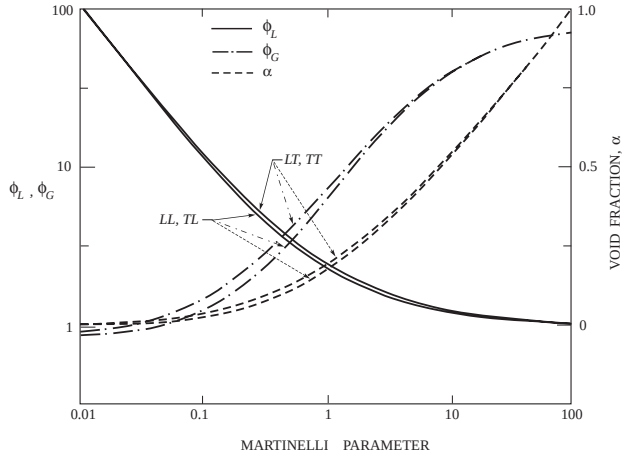

Figure 8.9. As figure 8.8 but for the annular flow case with $\kappa_L = 1/(1-\alpha)$ and $\kappa_G = 1$.

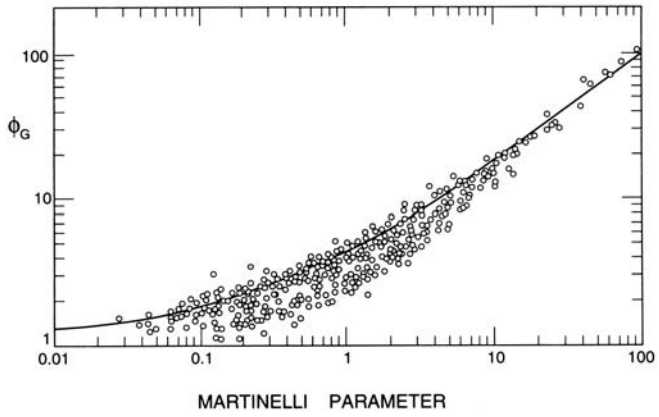

Figure 8.10. Comparison of the Lockhart-Martinelli correlation (the TT case) for ϕ_G (solid line) with experimental data. Adapted from Turner and Wallis (1965).

yield the individual mass fluxes, the mass quality and other flow properties. Alternatively one could begin the calculation with the mass quality rather than the void fraction and find the void fraction as one of the results. Finally the pressure gradient, dp/ds, follows from the values of ϕ_L^2 and ϕ_G^2.

The solutions for the cases $\kappa_L = \kappa_G = 1$ and $\kappa_L = 1/2(1-\alpha)$, $\kappa_G = 1$ are presented in figures 8.8 and 8.9 and the comparison of these two figures yields some measure of the sensitivity of the results to the flow geometry parameters, κ_L and κ_G. Similar charts are commonly used in the manner described

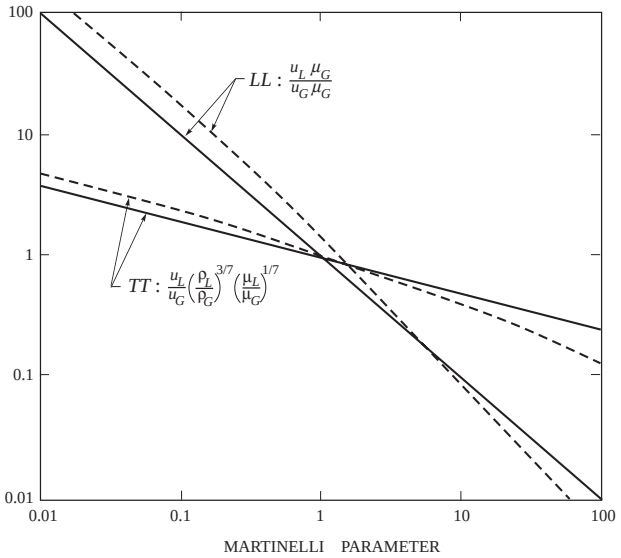

Figure 8.11. Ratios demonstrating the velocity ratio, u_L/u_G, implicit in the Lockhart-Martinelli correlation as functions of the Martinelli parameter, Ma, for the LL and TT cases. Solid lines: $\kappa_L = \kappa_G = 1$; dashed lines: $\kappa_L = 1/(1-\alpha)$, $\kappa_G = 1$.

above to obtain solutions for two-component gas/liquid flows in pipes. A typical comparison of the Lockhart-Martinelli prediction with the experimental data is presented in figure 8.10. Note that the scatter in the data is significant (about a factor of 3 in ϕ_G) and that the Lockhart-Martinelli prediction often yields an overestimate of the friction or pressure gradient. This is the result of the assumption that the entire perimeter of both phases experiences static wall friction. This is not the case and part of the perimeter of each phase is in contact with the other phase. If the interface is smooth this could result in a decrease in the friction; one the other hand a roughened interface could also result in increased interfacial friction.

It is important to recognize that there are many deficiencies in the Lockhart-Martinelli approach. First, it is assumed that the flow pattern consists of two parallel streams and any departure from this topology could result in substantial errors. In figure 8.11, the ratios of the velocities in the two streams which are implicit in the correlation (and follow from equation 8.19) are plotted against the Martinelli parameter. Note that large velocity differences appear to be predicted at void fractions close to unity. Since the flow is likely to transition to mist flow in this limit and since the relative velocities in the mist flow are unlikely to become large, it seems inevitable

that the correlation would become quite inaccurate at these high void fractions. Similar inaccuracies seem inevitable at low void fraction. Indeed, it appears that the Lockhart-Martinelli correlations work best under conditions that do not imply large velocity differences. Figure 8.11 demonstrates that smaller velocity differences are expected for turbulent flow (TT) and this is mirrored in better correlation with the experimental results in the turbulent flow case (Turner and Wallis 1965).

Second, there is the previously discussed deficiency regarding the suitability of assuming that the perimeters of both phases experience friction that is effectively equivalent to that of a static solid wall. A third source of error arises because the multiphase flows are often unsteady and this yields a multitude of quadratic interaction terms that contribute to the mean flow in the same way that Reynolds stress terms contribute to turbulent single phase flow.

8.3.2 Flow with phase change

The Lockhart-Martinelli correlation was extended by Martinelli and Nelson (1948) to include the effects of phase change. Since the individual mass fluxes are then changing as one moves down the pipe, it becomes convenient to use a different non-dimensional pressure gradient

$$\phi_{L0}^2 = \frac{\left(\frac{dp}{ds}\right)_{actual}}{\left(\frac{dp}{ds}\right)_{L0}} \tag{8.21}$$

where $(dp/ds)_{L0}$ is the hypothetical pressure gradient that would occur in the same pipe if a liquid flow with the same total mass flow were present. Such a definition is more practical in this case since the total mass flow is constant. It follows that ϕ_{L0}^2 is simply related to ϕ_L^2 by

$$\phi_{L0}^2 = (1-\mathcal{X})^{2-m_L}\phi_L^2 \tag{8.22}$$

The Martinelli-Nelson correlation uses the previously described Lockhart-Martinelli results to obtain ϕ_L^2 and, therefore, ϕ_{L0}^2 as functions of the mass quality, $\mathcal{X}$. Then the frictional component of the pressure gradient is given by

$$\left(-\frac{dp}{ds}\right)_{Frictional} = \phi_{L0}^2 \frac{2G^2\mathcal{K}_L}{\rho_L d}\left\{\frac{Gd}{\mu_L}\right\}^{-m_L} \tag{8.23}$$

Note that, though the other quantities in this expression for dp/ds are

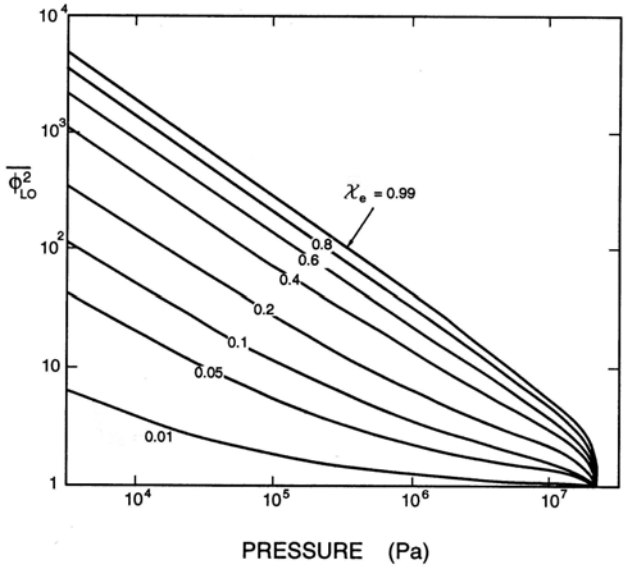

Figure 8.12. The Martinelli-Nelson frictional pressure drop function, $\overline{\phi^2_{L0}}$, for water as a function of the prevailing pressure level and the exit mass quality, $\mathcal{X}_e$. Case shown is for $\kappa_L = \kappa_G = 1.0$ and $m_L = m_G = 0.25$.

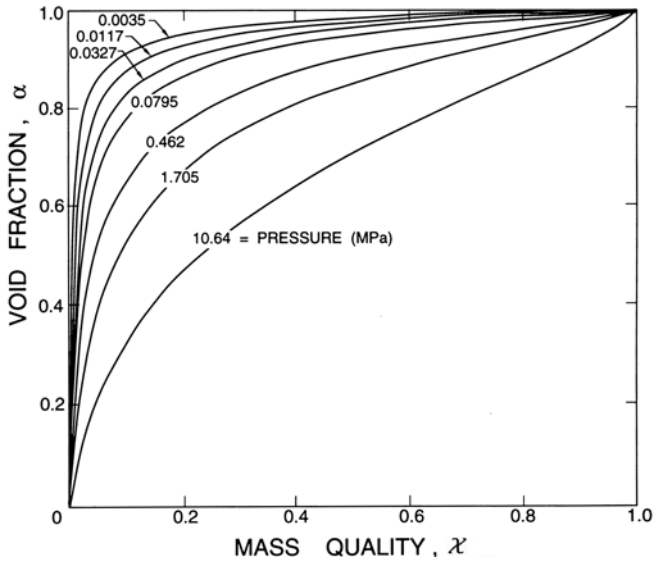

Figure 8.13. The exit void fraction values, α_e, corresponding to the data of figure 8.12. Case shown is for $\kappa_L = \kappa_G = 1.0$ and $m_L = m_G = 0.25$.

constant along the pipe, the quantity ϕ_{L0}^2 is necessarily a function of the mass quality, $\mathcal{X}$, and will therefore vary with s. It follows that to integrate equation 8.23 to find the pressure drop over a finite pipe length one must know the variation of the mass quality, $\mathcal{X}(s)$. Now, in many boilers, evaporators or condensers, the mass quality varies linearly with length, s, since

$$\frac{d\mathcal{X}}{ds} = \frac{\mathcal{Q}_\ell}{AG\mathcal{L}} \tag{8.24}$$

Since the rate of heat supply or removal per unit length of the pipe, $\mathcal{Q}_\ell$, is roughly uniform and the latent heat, $\mathcal{L}$, can be considered roughly constant, it follows that $d\mathcal{X}/ds$ is approximately constant. Then integration of equation 8.23 from the location at which $\mathcal{X} = 0$ to the location a distance, ℓ, along the pipe (at which $\mathcal{X} = \mathcal{X}_e$) yields

$$(\Delta p(\mathcal{X}_e))_{Frictional} = (p)_{\mathcal{X}=0} - (p)_{\mathcal{X}=\mathcal{X}_e} = \frac{2G^2\ell\mathcal{K}_L}{d\rho_L}\left\{\frac{Gd}{\mu_L}\right\}^{-m_L}\overline{\phi_{L0}^2} \tag{8.25}$$

where

$$\overline{\phi_{L0}^2} = \frac{1}{\mathcal{X}_e}\int_0^{\mathcal{X}_e}\phi_{L0}^2 d\mathcal{X} \tag{8.26}$$

Given a two-phase flow and assuming that the fluid properties can be estimated with reasonable accuracy by knowing the average pressure level of the flow and finding the saturated liquid and vapor densities and viscosities at that pressure, the results of the last section can be used to determine ϕ_{L0}^2 as a function of $\mathcal{X}$. Integration of this function yields the required values of $\overline{\phi_{L0}^2}$ as a function of the exit mass quality, $\mathcal{X}_e$, and the prevailing mean pressure level. Typical data for water are exhibited in figure 8.12 and the corresponding values of the exit void fraction, α_E, are shown in figure 8.13.

These non-dimensional results are used in a more general flow in the following way. If one wishes to determine the pressure drop for a flow with a non-zero inlet quality, $\mathcal{X}_i$, and an exit quality, $\mathcal{X}_e$, (or, equivalently, a given heat flux because of equation 8.24) then one simply uses figure 8.12, first, to determine the pressure difference between the hypothetical point upstream of the inlet at which $\mathcal{X} = 0$ and the inlet and, second, to determine the difference between the same hypothetical point and the outlet of the pipe.

But, in addition, to the frictional component of the pressure gradient there is also a contribution caused by the fact that the fluids will be accelerating due to the change in the mixture density caused by the phase change. Using the mixture momentum equation 1.50, it is readily shown that this

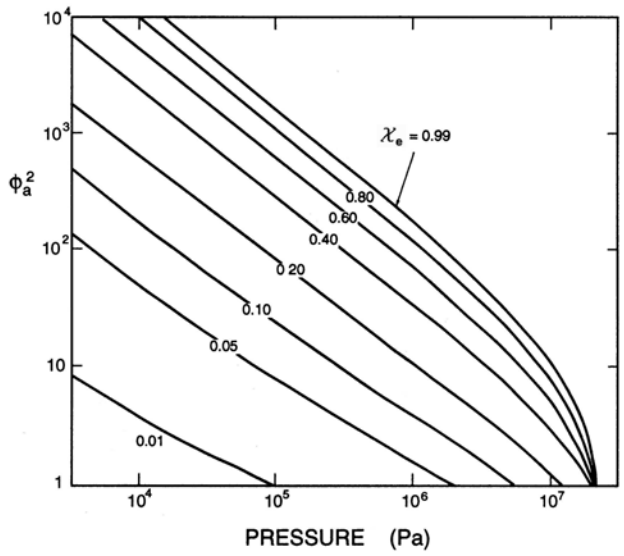

Figure 8.14. The Martinelli-Nelson acceleration pressure drop function, ϕ_a^2, for water as a function of the prevailing pressure level and the exit mass quality, $\mathcal{X}_e$. Case shown is for $\kappa_L = \kappa_G = 1.0$ and $m_L = m_G = 0.25$.

acceleration contribution to the pressure gradient can be written as

$$\left(-\frac{dp}{ds}\right)_{Acceleration} = G^2 \frac{d}{ds}\left\{\frac{\mathcal{X}^2}{\rho_G \alpha} + \frac{(1-\mathcal{X})^2}{\rho_L(1-\alpha)}\right\} \tag{8.27}$$

and this can be integrated over the same interval as was used for the frictional contribution to obtain

$$(\Delta p(\mathcal{X}_e))_{Acceleration} = G^2 \rho_L \phi_a^2(\mathcal{X}_e) \tag{8.28}$$

where

$$\phi_a^2(\mathcal{X}_e) = \left\{\frac{\rho_L \mathcal{X}_e^2}{\rho_G \alpha_e} + \frac{(1-\mathcal{X}_e)^2}{(1-\alpha_e)} - 1\right\} \tag{8.29}$$

As in the case of $\overline{\phi_{L0}^2}$, $\phi_a^2(\mathcal{X}_e)$ can readily be calculated for a particular fluid given the prevailing pressure. Typical values for water are presented in figure 8.14. This figure is used in a manner analogous to figure 8.12 so that, taken together, they allow prediction of both the frictional and acceleration components of the pressure drop in a two-phase pipe flow with phase change.

8.4 ENERGY CONVERSION IN PUMPS AND TURBINES

Apart from pipes, most pneumatic or hydraulic systems also involve a whole collection of components such as valves, pumps, turbines, heat exchangers, etc. The flows in these devices are often complicated and frequently require highly specialized analyses. However, effective single phase analyses (homogeneous flow analyses) can also yield useful results and we illustrate this here by reference to work on the multiphase flow through rotating impeller pumps (centrifugal, mixed or axial pumps).

8.4.1 Multiphase flows in pumps

Consistent with the usual turbomachinery conventions, the total pressure increase (or decrease) across a pump (or turbine) and the total volumetric flux (based on the discharge area, A_d) are denoted by Δp^T and j, respectively, and these quantities are non-dimensionalized to form the head and flow coefficients, ψ and ϕ, for the machine:

$$\psi = \frac{\Delta p^T}{\rho \Omega^2 r_d^2} \quad ; \quad \phi = \frac{j}{\Omega r_d} \tag{8.30}$$

where Ω and r_d are the rotating speed (in radians/second) and the radius of the impeller discharge respectively and ρ is the mixture density. We note that sometimes in presenting cavitation performance, the impeller inlet area, A_i, is used rather than A_d in defining j, and this leads to a modified flow coefficient based on that inlet area.

The typical centrifugal pump performance with multiphase mixtures is exemplified by figures 8.15, 8.16 and 8.17. Figure 8.15 from Herbich (1975) presents the performance of a centrifugal dredge pump ingesting silt/clay/water mixtures with mixture densities, ρ, up to $1380 kg/m^3$. The corresponding solids fractions therefore range up to about 25% and the figure indicates that, provided ψ is defined using the mixture density, there is little change in the performance even up to such high solids fractions. Herbich also shows that the silt and clay suspensions cause little change in the equivalent homogeneous cavitation performance of the pump.

Data on the same centrifugal pump with air/water mixtures of different volume quality, β, is included in figure 8.16 (Herbich 1975). Again, there is little difference between the multiphase flow performance and the homogeneous flow prediction at small discharge qualities. However, unlike the solids/liquid case, the air/water performance begins to decline precipitously above some critical volume fraction of gas, in this case a volume fraction con-

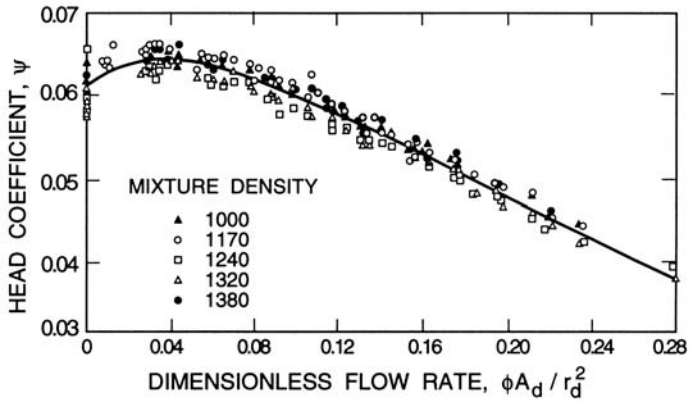

Figure 8.15. The head coefficient, ψ, for a centrifugal dredge pump ingesting silt/clay/water mixtures plotted against a non-dimensional flow rate, $\phi A_d/r_d^2$, for various mixture densities (in kg/m^3). Adapted from Herbich (1975).

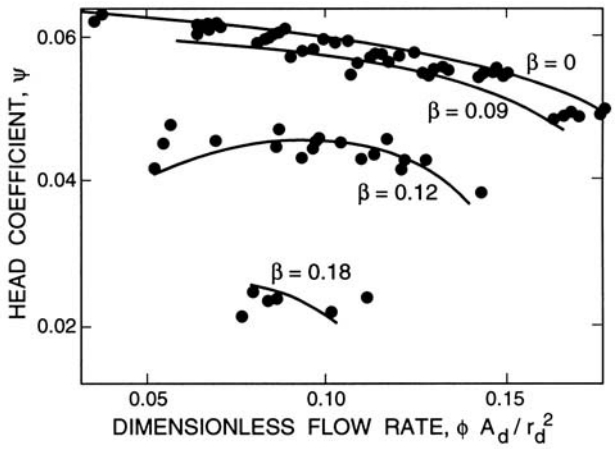

Figure 8.16. The head coefficient, ψ, for a centrifugal dredge pump ingesting air/water mixtures plotted against a non-dimensional flow rate, $\phi A_d/r_d^2$, for various volumetric qualities, β. Adapted from Herbich (1975).

sistent with a discharge quality of about 9%. Below this critical value, the homogeneous theory works well; larger volumetric qualities of air produce substantial degradation in performance.

Patel and Runstadler (1978), Murakami and Minemura (1978) and many others present similar data for pumps ingesting air/water and steam/water mixtures. Figure 8.17 presents another example of the air/water flow through a centrifugal pump. In this case the critical inlet volumetric quality is only

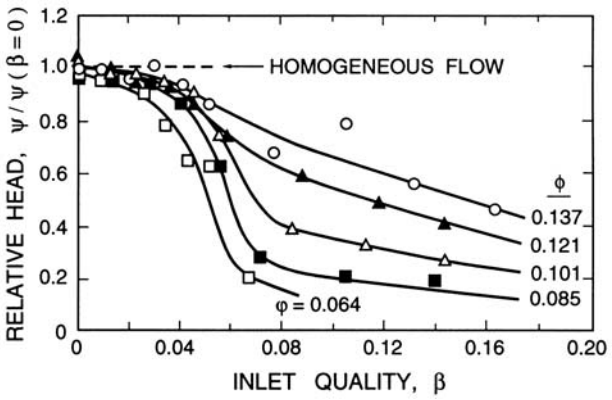

Figure 8.17. The ratio of the pump head with air/water mixtures to the head with water alone, $\psi/\psi(\beta = 0)$, as a function of the inlet volumetric quality, β, for various flow coefficients, ϕ. Data from Patel and Runstadler (1978) for a centrifugal pump.

about $\beta = 3\%$ or 4% and the degradation appears to occur at lower volume fractions for lower flow coefficients. Murakami and Minemura (1978) obtained similar data for both axial and centrifugal pumps, though the performance of axial flow pumps appear to fall off at even lower air contents.

A qualitatively similar, precipitous decline in performance occurs in single phase liquid pumping when cavitation at the inlet to the pump becomes sufficiently extensive. This performance degradation is normally presented dimensionlessly by plotting the head coefficient, ψ, at a given, fixed flow coefficient against a dimensionless inlet pressure, namely the cavitation number, σ (see section 5.2.1), defined as

$$\sigma = \frac{(p_i - p_V)}{\frac{1}{2}\rho_L \Omega^2 r_i^2} \tag{8.31}$$

where p_i and r_i are the inlet pressure and impeller tip radius and p_V is the vapor pressure. An example is shown in figure 8.18 which presents the cavitation performance of a typical centrifugal pump. Note that the performance declines rapidly below a critical cavitation number that usually corresponds to a fairly high vapor volume fraction at the pump inlet.

There appear to be two possible explanations for the decline in performance in gas/liquid flows above a critical volume fraction. The first possible cause, propounded by Murakami and Minemura (1977,1978), Patel and Runstadler (1978), Furuya (1985) and others, is that, when the void fraction exceeds some critical value the flow in the blade passages of the pump becomes stratified because of the large crossflow pressure gradients. This

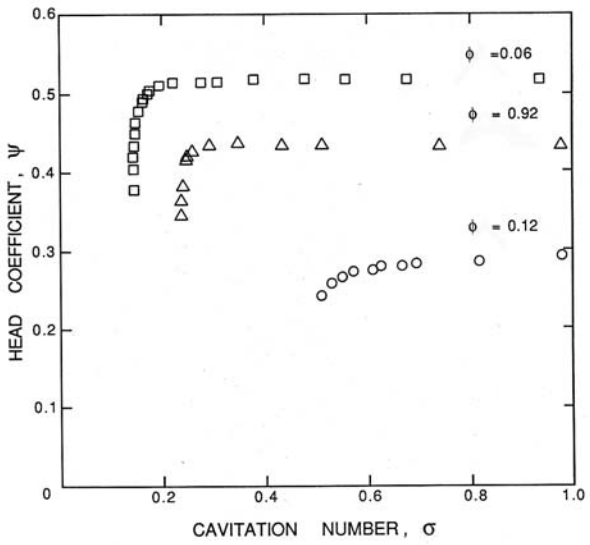

Figure 8.18. Cavitation performance for a typical centrifugal pump (Franz *et al.* 1990) for three different flow coefficients, ϕ

allows a substantial deviation angle to develop at the pump discharge and, as in conventional single phase turbomachinery analyses (Brennen 1994), an increasing deviation angle implies a decline in performance. The lower critical volume fractions at lower flow coefficients would be consistent with this explanation since the pertinent pressure gradients will increase as the loading on the blades increases. Previously, in section 7.3.3, we discussed the data on the bubble size in the blade passages compiled by Murakami and Minemura (1977, 1978). Bubble size is critical to the process of stratification since larger bubbles have larger relative velocities and will therefore lead more readily to stratification. But the size of bubbles in the blade passages of a pump is usually determined by the high shear rates to which the inlet flow is subjected and therefore the phenomenon has two key processes, namely shear at inlet that determines bubble size and segregation in the blade passages that governs performance.

The second explanation (and the one most often put forward to explain cavitation performance degradation) is based on the observation that the vapor (or gas) bubbles grow substantially as they enter the pump and subsequently collapse as they are convected into regions of higher pressure within the blade passages of the pump. The displacement of liquid by this volume growth and collapse introduces an additional flow area restriction into the flow, an additional inlet *nozzle* caused by the cavitation. Stripling and Acosta

(1962) and others have suggested that the head degradation due to cavitation could be due to a lack of pressure recovery in this effective additional nozzle.